Applied Physics Letters

RESEARCH ARTICLE | APRIL 24 2023

Nonlinear chiral magnonic resonators: Toward magnonic neurons

K. G. Fripp; Y. Au; A. V. Shytov; ... et. al

Check for updates

Appl. Phys. Lett. 122, 172403 (2023)
https://doi.org/10.1063/5.0149466

View Online
Export Citation
CrossMark

Downloaded from http://pubs.aip.org/aip/apl/article-pdf/doi/10.1063/5.0149466/16967078/172403_1_5.0149466.pdf

AIP Publishing

Applied Physics Letters ARTICLE scitation.org/journal/apl

Nonlinear chiral magnonic resonators: Toward magnonic neurons

Cite as: Appl. Phys. Lett. **122**, 172403 (2023); doi: 10.1063/5.0149466
Submitted: 6 March 2023 · Accepted: 9 April 2023 ·
Published Online: 24 April 2023

View Online Export Citation CrossMark

K. G. Fripp, Y. Au, A. V. Shytov, and V. V. Kruglyak[a)]

AFFILIATIONS

University of Exeter, Stocker Road, Exeter EX4 4QL, United Kingdom

[a)]Author to whom correspondence should be addressed: V.V.Kruglyak@exeter.ac.uk

ABSTRACT

We explore chiral magnonic resonators as building blocks of artificial neural networks. Via micromagnetic simulations and analytical modeling, we demonstrate that the spin-wave modes confined in the resonators exhibit a strongly nonlinear response owing to energy concentration when resonantly excited by incoming spin waves. This effect may be harnessed to implement an artificial neuron in a network. Therefore, the confined and propagating spin-wave modes can serve as neurons and interneural connections, respectively. For modest excitation levels, the effect can be described in terms of a nonlinear shift of the resonant frequency ("detuning"), which results in amplitude-dependent transmission of monochromatic spin waves, which may be harnessed to recreate a "sigmoid-like" activation function. At even stronger excitation levels, the nonlinearity leads to bistability and hysteresis, akin to those occurring in nonlinear oscillators when the excitation strength exceeds a threshold set by the decay rate of the mode. In magnonic resonators, the latter includes both the Gilbert damping and the radiative decay due to the coupling with the medium. The results of our simulations are well described by a phenomenological model in which the nonlinear detuning of the confined mode is quadratic in its amplitude, while the propagation in the medium is linear.

© 2023 Author(s). All article content, except where otherwise noted, is licensed under a Creative Commons Attribution (CC BY) license (http://creativecommons.org/licenses/by/4.0/). https://doi.org/10.1063/5.0149466

Artificial intelligence and neuromorphic computing are the major areas of recent expansion of magnonics,[1] in its search for a technology niche where the use of spin waves[2] could yield decisive practical benefits.[3–5] Hence, the research focus in magnonics is shifting from the design and demonstration of individual devices and functionalities[6–18] to exploration and exploitation of more complex systems and approaches that could benefit from the power of machine learning.[19–21] This includes devices that exploit resonant coupling between propagating and confined spin-wave modes.[6,8,11–16,18] In Ref. 16, chiral magnonic resonators[6,7,12,14] (Fig. 1) are proposed as building blocks of artificial neural networks. The idea is that the confined and propagating spin-wave modes would serve as neurons and interneural connections, respectively, and that the resonant increase in the confined modes' amplitude would bolster their nonlinearity and, thereby, also the computing power of the whole neural network. However, the nonlinearity of chiral magnonic resonators has not been systematically explored, a gap bridged here.

We use micromagnetic simulations and phenomenological modeling to study the nonlinear behavior of stripe chiral magnonic resonators[14] in view of their potential use as artificial neurons. We show that, at moderately strong excitation levels, a nonlinear shift of the confined mode frequency leads to an amplitude-dependent transmission of the propagating spin wave at a fixed frequency. We demonstrate that this amplitude-dependent transmission mimics the thresholding behavior of an artificial neuron. At even stronger excitation levels, the phenomena of bistability and hysteresis are observed in the spin-wave transmission curves. The simulated data are fitted using a phenomenological model, obtained by including the cubic nonlinearity of the resonator's local mode but keeping the propagating modes linear. Our results are consistent both with those for other nonlinear magnonic systems and with predictions of the more general theory of nonlinear oscillations.

To characterize the amplitude dependence of the transmission coefficient of the stripe chiral magnonic resonator [Fig. 1(a)], we use numerical micromagnetic simulations run with MuMax3.[22] The resonator is represented by a magnetic stripe placed 15 nm beneath a magnonic waveguide. The resonator and waveguide are both assumed infinite in the y-direction but have $x \times z$ cross-sectional dimensions of 50×20 and $10\,240 \times 20\ \mathrm{nm}^2$, respectively. Their infinite extent is simulated using the periodic boundary conditions in the macro-geometry approximation, with the macro-geometry having a square shape in the (x, y) plane. The sample is discretized into 5 nm cubic cells. The

Downloaded from http://pubs.aip.org/aip/apl/article-pdf/doi/10.1063/5.0149466/16967078/172403_1_5.0149466.pdf

© Author(s) 2023

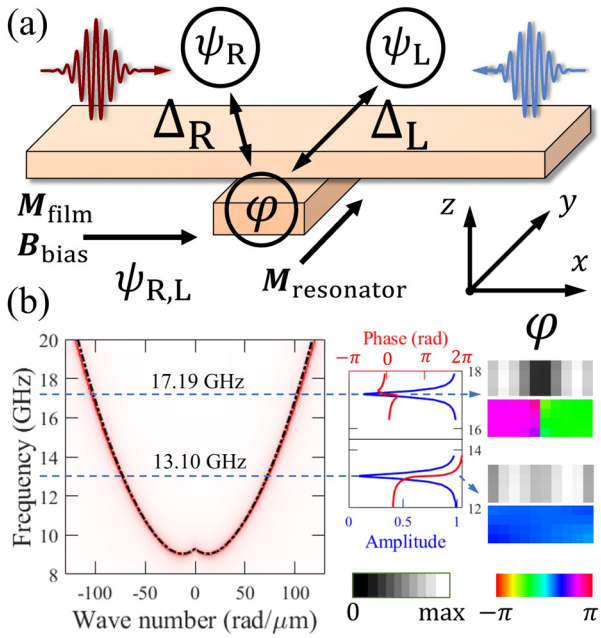

FIG. 1. (a) A stripe chiral magnonic resonator under a magnonic waveguide is shown. The waveguide's magnetization, $\boldsymbol{M}_{\text{film}} \parallel \hat{\boldsymbol{x}}$, is aligned by the bias field, $\boldsymbol{B}_{\text{bias}}$, while the resonator's magnetization, $\boldsymbol{M}_{\text{resonator}} \parallel \hat{\boldsymbol{y}}$, is aligned by its shape anisotropy. The resonator's local mode, $\varphi(t)$, is coupled, with coupling strengths Δ_R and Δ_L, to propagating modes of the waveguide: right-going $\psi_R(t,x)$ and left-going $\psi_L(t,x)$, respectively. (b) The left panel shows the dispersion of backward-volume spin waves in an isolated waveguide: The analytical result (black dashed line) is overlaid on the simulated data (red background). The center panel shows the linear transmission of right-going waves computed numerically for a chiral magnonic resonator located 15 nm below the waveguide. The right panel shows the simulated (x,z) distributions of the Fourier amplitude (top) and phase (bottom) of the resonator's quasi-uniform and dark modes, corresponding to the transmission dips at 13.1 and 17.19 GHz, respectively.

waveguide and resonator have identical magnetic parameters: the saturation magnetization, M_S, of 800 kA/m, the exchange constant of 13 pJ/m, zero magneto-crystalline anisotropy, the Gilbert damping constant of 0.005, and the default value of the gyromagnetic ratio. The 2.5 μm regions near the waveguide's ends have their Gilbert damping increased to 0.1, to suppress spin-wave reflections. A bias magnetic field of 100 mT magnetizes the waveguide in the x direction—that of spin-wave propagation. This yields the spin-wave dispersion [Fig. 1(b)] typical for the backward volume geometry, as in Refs. 6, 7, and 14, and we avoid complications associated with non-reciprocity of the Damon–Eshbach configuration and with quantization in patterned waveguides. We note that, however, the effects described below should persist for all types of spin waves, including those in the Damon–Eshbach and forward volume configurations.[5,14,16] No bias magnetic field is applied to the stripe resonator, whose magnetization is aligned along the y-direction by its shape anisotropy.

In the dynamic simulations, right-going monochromatic spin waves are launched by a magnetic field, $\boldsymbol{b}_{\text{ext}}(x,t) \parallel \hat{\boldsymbol{z}}$. The field is uniform in the (y,z) plane and Gaussian-shaped in the x-direction, with the Gaussian centered at the boundary between the regions of increased and normal damping near the waveguide's left end. The field is harmonic with its amplitude ramped up from zero to the set value b_0 over time of about 2 ns. The time evolution of the magnetization is sampled eight times per period of the driving field over 32 ns, which enables us to resolve any second and third harmonic generation without Fourier aliasing and, with appropriate windowing and zero-padding,[14] to exclude the long-duration transient effects. The transmission coefficient τ_R is computed using[14]

$$\tau_R = \left[\sum_S \frac{\mathcal{F}\{M_z\}_\omega}{\mathcal{F}\{M_z^{\text{ref}}\}_\omega} \right]^*, \tag{1}$$

where ω is the angular frequency; $\mathcal{F}\{\}_\omega$ denotes the Fourier transform from the time to frequency domain; M_z and M_z^{ref} are z-components the waveguide's magnetization in simulations with and without the resonator, respectively; $\sum_S$ denotes averaging over the (y,z) cross section of the waveguide at a distance of 1 μm to the right from the resonator; and the asterisk denotes complex conjugation.

Figure 2 shows the frequency dependence of the transmission coefficient τ_R computed for different excitation strengths, for frequencies near the quasi-uniform [Fig. 2(a)] and dark [Fig. 2(b)] modes. As the amplitude A_0 of the incident spin wave increases, the transmission minima shift to lower frequencies, and the transmission line shapes develop asymmetry. In particular, the left-hand slope becomes nearly vertical for amplitudes A_0 above 0.031 M_S. This behavior is consistent with the transition to the bistable regime (well-studied for other magnonic systems e.g., in Refs. 11 and 23–27) that manifests itself as a hysteresis when the frequency is swept ("chirped") in the vicinity of the resonance. To simulate the hysteresis, the constant excitation frequency, f, is replaced by a linearly chirped one, defined as

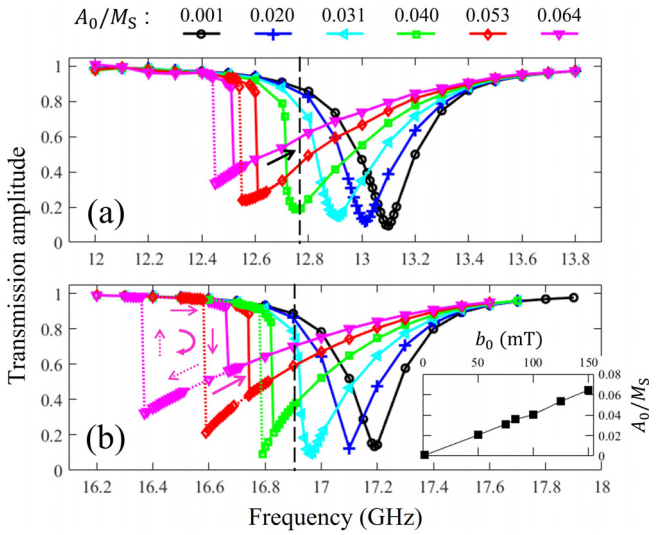

FIG. 2. The transmission amplitude, $|\tau_R|$, is shown for spin-wave frequencies near the quasi-uniform (a) and dark (b) modes, for different incident wave amplitudes, A_0. In the regime of bistability, the dotted lines indicate the alternative transmission branch, and the arrows indicate the path of the hysteresis evolution when cycling the frequency. The dashed lines indicate the critical frequency, below which the bistability occurs. The inset in (b) shows the relationship between the driving field strength b_0 and the A_0/M_S ratio at the waveguide location corresponding to the midpoint of the resonator, obtained from the reference simulations.

Downloaded from http://pubs.aip.org/aip/apl/article-pdf/doi/10.1063/5.0149466/16967078/172403_1_5.0149466.pdf

© Author(s) 2023

$2\pi f(t) = d\phi(t)/dt$. Here, the phase varies as $\phi(t) = 2\pi(\frac{\Delta f}{2T}t^2 + f_0 t)$, where Δf is the overall frequency change (from the initial value f_0) over chirping duration $T = 80$ ns, long enough to make the transition smooth. The transmission for each metastable state is computed from simulations run for another 32 ns while keeping the excitation strength and frequency constant. The simulations reproduce the bistability expected at amplitudes above 0.031 M_S, revealing regimes of high and low transmissions when sweeping the incident spin-wave frequency up and down, respectively. The full transmission hysteresis loop is accessed in the clockwise direction, as shown by arrows in Fig. 2(b).

The inset in Fig. 2(b) (also Fig. S1 of the supplementary material) shows that the spin waves in the waveguide remain in the linear regime when their transmission spectra already exhibit a strong nonlinearity. The latter is, therefore, associated with the nonlinearity of the resonator's modes. This corroborates the speculations from Ref. 16 of using chiral magnonic resonators as building blocks of artificial neural networks and their modes as magnonic neurons. Furthermore, this observation supports our earlier conjecture that propagating spin waves could serve as linear interneural connections and the magnonic waveguides could, therefore, work as artificial synapses.[28] The strong nonlinearity confined to the resonators distinguishes our system from those in Refs. 11, 19, 20, and 27, which exploited nonlinearity of propagating modes.

From the viewpoint of designing devices for neuromorphic computing, the possibility of replicating a sigmoid-like activation function from the resonator's response would be of particular interest. This is demonstrated in Fig. 3 for the spin-wave frequency tuned to the transmission minimum in the linear regime. The nonlinear detuning of the minimum (Fig. 2) enhances the transmission, for both the quasi-uniform and dark modes. However, the amplitude dependence of the transmission coefficient is modified drastically as the frequency of the incident spin waves changes by as little as 100 MHz. This could present a limitation for computing schemes exploiting time- or

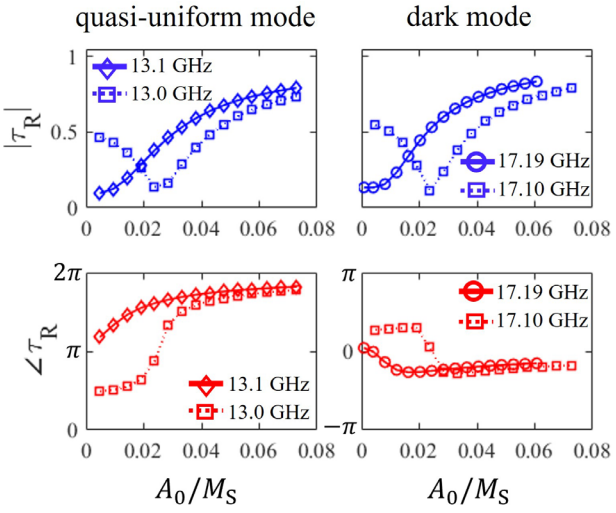

FIG. 3. The dependence of the magnitude (top row) and phase (bottom row) of the transmission coefficient, τ_R, upon the amplitude of the incident spin waves, A_0/M_S, is illustrated for wave frequencies near the quasi-uniform (left column) and dark (right column) mode resonances. The curves at 13.1 and 17.19 GHz show a sigmoid-like activation function response. The curves at 13 and 17.1 GHz show the behavior of a power limiter.

frequency-domain multiplexing[19] albeit not for those using space multiplexing.[20] Alternatively, such resonators showing a reduced transmission at increased spin-wave amplitudes could find an application as power limiters. The individual characteristics (beyond the frequency difference) of the resonator's quasi-uniform and dark modes may play a role when selecting one of them for applications: e.g., the enhanced non-reciprocity and suppressed reflection of the dark mode[14] can be advantageous for resonators placed in series. It is apparent, however, that for both modes, the transmission never reaches 100% regardless of the amplitude of the incident spin wave. This will limit the number of resonators that can be concatenated, unless spin-wave amplifiers are used between successive resonators to compensate losses due to both the unwanted absorption/reflection in the resonator and the Gilbert damping in the waveguide. Alternatively, one could make the resonator using low-damping materials like yttrium-iron garnet (YIG).[29] This would reduce the intrinsic linewidth, Γ_0, of the resonator (compared to the Permalloy resonator studied here), making the transmission dips in Fig. 2 narrower and resulting in a stronger transmission at the same nonlinear detuning from the resonance. Furthermore, the nonlinearity would be expected to manifest at even lower spin-wave amplitudes. The shape (i.e., minima, maxima, and "steepness") of the response in Fig. 3 can also be controlled by choice of the resonator's cross section, waveguide-to-resonator spacing, and the strength and orientation of the bias magnetic field.[6,14,16]

In Ref. 14, we introduced a phenomenological model for chiral resonant scattering of spin waves, which we now extend to the nonlinear regime. In the model, the local mode, $\varphi(t)$, is represented as an oscillator of resonant frequency Ω_0 and decrement Γ_0 linearly coupled to the propagating left- and right-moving waves. To describe our findings, we incorporate the nonlinearity in the dynamics of the oscillator. In principle, this can be done in many ways, e.g., by introducing new terms in the equation for the oscillator, which can be quadratic, cubic, or higher-order in either displacement or velocity of the mode. However, from the theory of nonlinear oscillations,[30,31] it is well-known that, if the system is probed near the resonance, the primary effect is the shift of the resonant frequency. For a cubic nonlinearity, this shift is quadratic in amplitude and may be positive or negative in sign. For a quadratic nonlinearity, the shift is also quadratic but always negative. Consequently, the behavior near the resonance is rather universal and is not tied to a specific form of the nonlinear contributions. Indeed, let us consider free motion of the system without damping. In the linear regime, it is sinusoidal with amplitude-independent frequency. Nonlinear effects deform it into a periodic motion of a more complicated shape, e.g., by clipping the sine wave. However, such deformations are projected away when the fundamental harmonic is extracted from the signal, and the nonlinearity is only manifested in the link between the period and the amplitude. Hence, nonlinearities of different types are best distinguished in other effects, such as rectification and higher harmonic generation, which are beyond the scope of our analysis. Thus, we describe the local mode, $\varphi(t)$, via the following equation:

$$i\frac{\partial\varphi(t)}{\partial t} = (\Omega_0 - i\Gamma_0)\varphi(t) - \lambda|\varphi(t)|^2\varphi(t) + \Delta_R^*\psi_R(t,0) + \Delta_L^*\psi_L(t,0). \quad (2)$$

The first term describes a free linear oscillator of frequency Ω_0 and dissipative linewidth Γ_0. The second term introduces the nonlinearity λ via the quadratic shift of the resonant frequency:

Downloaded from http://pubs.aip.org/aip/apl/article-pdf/doi/10.1063/5.0149466/16967078/172403_1_5.0149466.pdf

© Author(s) 2023

$$\omega_{\rm res} = \Omega_0 - \lambda|\varphi|^2. \tag{3}$$

The remaining terms describe hybridization with the right-going wave $\psi_{\rm R}(t,x)$ and left-going wave $\psi_{\rm L}(t,x)$, where $\Delta_{\rm R}$ and $\Delta_{\rm L}$ are the respective coupling strengths, at the resonator's position $x = 0$. Based on our earlier observations, we keep the equations describing the right-going wave $\psi_{\rm R}(t,x)$ and left-going wave $\psi_{\rm L}(t,x)$ linear,

$$\begin{aligned} \frac{\partial\psi_{\rm R}(t,x)}{\partial t} + v_{\rm R}\frac{\partial\psi_{\rm R}(t,x)}{\partial x} &= -i\delta(x)\Delta_{\rm R}\,\varphi(t), \\ \frac{\partial\psi_{\rm L}(t,x)}{\partial t} - v_{\rm L}\frac{\partial\psi_{\rm L}(t,x)}{\partial x} &= -i\delta(x)\Delta_{\rm L}\,\varphi(t), \end{aligned} \tag{4}$$

where $v_{\rm R(L)}$ is the group velocity of the local mode to the right (left) propagating modes.

Integrating Eq. (4) along x (as in Ref. 14) and denoting the complex amplitude of the incident spin wave at $x = 0$ as I, we obtain for the transmission coefficient

$$\tau_{\rm R(L)} = 1 - \frac{i\Delta^*_{\rm R(L)}}{v_{\rm R(L)}}\frac{\varphi}{I}, \tag{5}$$

where the local mode of the driven nonlinear harmonic oscillator is described by

$$i\frac{\partial\varphi}{\partial t} = (\Omega_0 - i\Gamma_{\rm tot})\varphi - \lambda|\varphi|^2\varphi + \Delta_{\rm R}I. \tag{6}$$

Here, the resonator's total linewidth is $\Gamma_{\rm tot} = \Gamma_0 + \Gamma_{\rm R} + \Gamma_{\rm L}$, where $\Gamma_{\rm R(L)} \equiv |\Delta_{\rm R(L)}|^2/(2v_{\rm R(L)})$ are its radiative linewidths into the right (left) propagating mode. The reflection coefficient is

$$r_{\rm R(L)} = -\frac{i\Delta^*_{\rm L(R)}}{v_{\rm L(R)}}\frac{\varphi}{I}. \tag{7}$$

To apply this theory to our data, we note that the modes φ and ψ are proportional to the magnetization disturbances in the resonator and in the waveguide, with normalization coefficients that depend upon the volume of the resonator, width of the waveguide, and other parameters. However, we are interested in the nonlinear frequency shift and its effect on the transmission, rather than the modes φ and ψ *per se*. Therefore, we simplify the analysis by rescaling φ and I and recasting Eq. (6), for excitation at frequency ω, in the form involving only the magnitude $|\tilde{\varphi}|$ of the rescaled local mode

$$[(\omega - \Omega_0 + \tilde{\lambda}|\tilde{\varphi}|^2)^2 + \Gamma_{\rm tot}^2]|\tilde{\varphi}|^2 = |A_0|^2. \tag{8}$$

We do this to eliminate the factor of Δ_R on the right-hand side as well as the proportionality coefficient between I and A_0. The rescaling only affects the coefficient in the nonlinear term, denoted as $\tilde{\lambda}$, but does not change the overall frequency shift: $\lambda|\varphi|^2 = \tilde{\lambda}|\tilde{\varphi}|^2$. Thus, the frequency shift is found from a cubic in $|\tilde{\varphi}|^2$ equation with only one unknown parameter $\tilde{\lambda}$. Depending on the values of the amplitude A_0 and frequency ω of the incident spin wave, the equation has either one or three real roots. Once $|\tilde{\varphi}|^2$ is found, the amplitude-dependent transmission coefficient is calculated as in linear theory with a shifted resonance frequency,

$$\tau_{\rm R}(\omega, |A_0|) = \frac{\omega - \Omega_0 + \tilde{\lambda}|\tilde{\varphi}|^2 + i(\Gamma_{\rm tot} - 2\Gamma_{\rm R})}{\omega - \Omega_0 + \tilde{\lambda}|\tilde{\varphi}|^2 + i\Gamma_{\rm tot}}. \tag{9}$$

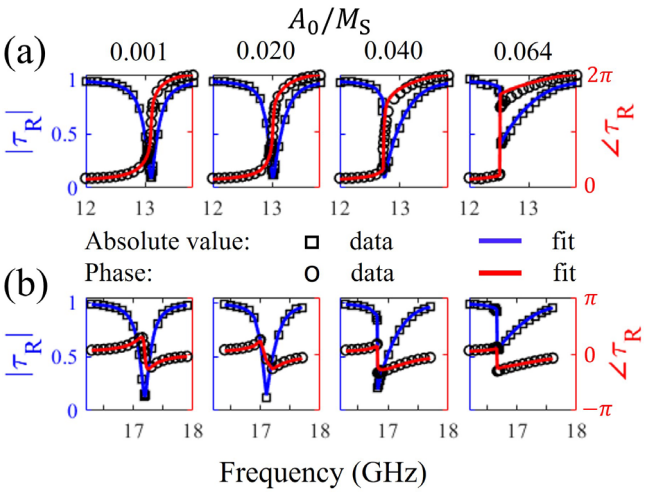

FIG. 4. The amplitude and phase of the simulated transmission (symbols) and corresponding fits to the phenomenological model (lines) are shown for different spin-wave amplitudes and frequencies near the resonator's (a) quasi-uniform and (b) dark mode.

The existence of multiple roots is responsible for the bistability observed in Fig. 2 and directly related to the foldover effect in nonlinear ferromagnetic resonance.[23–26] The bistable regime may only occur if the incident spin wave's frequency is below a critical value,

$$\omega' = \Omega_0 - \Gamma_{\rm tot}\sqrt{3}. \tag{10}$$

The corresponding values of the propagating and local modes' amplitudes are given by

$$|A_0'| = \frac{2\sqrt{2}}{3^{3/4}}\sqrt{\frac{\Gamma_{\rm tot}^3}{\tilde{\lambda}}} \quad \text{and} \quad |\tilde{\varphi}'| = \frac{\sqrt{2}}{3^{1/4}}\sqrt{\frac{\Gamma_{\rm tot}}{\tilde{\lambda}}}, \tag{11}$$

respectively, both of which can be used to identify the nonlinear parameter $\tilde{\lambda}$.

Figure 4 presents results of fitting the simulated data from Fig. 2 to the phenomenological model. The simulated complex transmission coefficient is fitted to

$$\tau_{\rm fit} = \tau_{\rm R}\exp(i\Phi_{\rm R}), \tag{12}$$

where $\tau_{\rm R}$ is defined by Eq. (9) with $|\tilde{\varphi}|^2$ found from Eq. (8). As in Ref. 14, the phase factor $\exp(i\Phi_{\rm R})$ is included to offset effects associated with the finite precision of the simulations and presence of additional resonator modes (not accounted for in the model). The following procedure is used. First, the data at $A_0/M_S = 0.001$ are fitted to the linear model, to obtain the values of Ω_0, $\Gamma_0 + \Gamma_{\rm L}$, $\Gamma_{\rm R}$, and $\Phi_{\rm R}$ (Table I).

TABLE I. The parameters extracted from the fit of the simulated data at $A_0/M_S = 0.001$ to the phenomenological model with zero λ are shown.

Mode	$\frac{\Omega_0}{2\pi}$ (GHz)	$\frac{\Gamma_0+\Gamma_{\rm L}}{2\pi}$ (GHz)	$\frac{\Gamma_{\rm R}}{2\pi}$ (GHz)	$\Phi_{\rm R}$ (rad)
Quasi-uniform	13.10	0.0863	0.1038	0.290
Dark	17.19	0.0893	0.0688	0.050

Downloaded from http://pubs.aip.org/aip/apl/article-pdf/doi/10.1063/5.0149466/16967078/172403_1_5.0149466.pdf

© Author(s) 2023

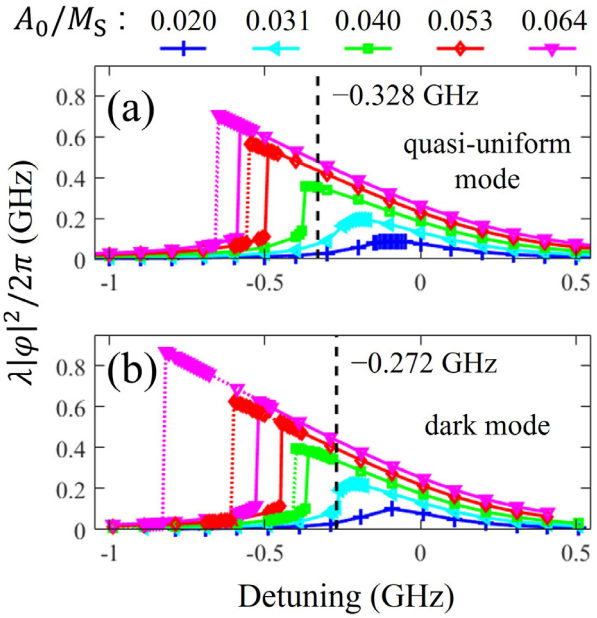

FIG. 5. The nonlinear resonance frequency shift, $\lambda|\varphi|^2$, is shown as a function of detuning from the linear resonance frequency, $\frac{\omega-\Omega_0}{2\pi}$, for different spin-wave amplitudes and frequencies near the resonator's (a) quasi-uniform and (b) dark mode. The vertical dashed lines correspond to the critical frequency $\frac{\omega'}{2\pi}$.

With these values fixed, the value of $\tilde{\lambda}$ is then used as the only fitting parameter when fitting datasets for A_0/M_S values of 0.02, 0.04, and 0.064, representing cases of "weak," "moderate," and "strong" nonlinearity, respectively. The best agreement is found for $\tilde{\lambda} = 9 \times 10^{-10}$ GHz m^2 A^{-2}, for both resonator modes. Figure 5 shows the nonlinear resonance frequency shift, $\lambda|\varphi|^2$, found for different excitation strengths using the parameters extracted from the fits. The parameter values from Table I are used to plot the vertical dashed lines corresponding to the critical frequency ω'. At frequencies below the critical value, the foldover is observed, as expected.

In summary, we have modeled spin-wave scattering from a nonlinear chiral magnonic resonator. At moderately strong excitation levels, the nonlinear resonance detuning (resonance frequency shift) is observed, which results in an amplitude-dependent transmission at a fixed spin-wave frequency. We show that this amplitude-dependent transmission may be harnessed to recreate the thresholding behavior of an artificial neuron. At even stronger excitation levels, the phenomena of bistability and hysteresis are observed in the transmission curves, related to the foldover of the nonlinear resonance curve of the resonator's local modes. The simulated data are fitted well using a phenomenological model, obtained by including the cubic nonlinearity of the resonator's local mode but keeping the propagating modes linear. Our results are consistent both with those for other nonlinear magnonic systems and with predictions of the more general theory of nonlinear oscillations.

See the supplementary material for spatial profiles of spin waves propagating in the magnonic waveguide for different excitation strengths.

The research leading to these results has received funding from the UK Research and Innovation (UKRI) under the UK government's Horizon Europe funding guarantee (Grant No. 10039217) as part of the Horizon Europe (HORIZON-CL4-2021-DIGITAL-EMERGING-01) under Grant Agreement No. 101070347 and from EPSRC of the UK (Project Nos. EP/L019876/1 and EP/T016574/1).

AUTHOR DECLARATIONS

Conflict of Interest

The authors have no conflicts to disclose.

Author Contributions

Kevin G. Fripp: Data curation (lead); Formal analysis (equal); Investigation (equal); Methodology (equal); Software (lead); Validation (equal); Visualization (lead); Writing – original draft (equal); Writing – review & editing (supporting). **Yat-Yin Au:** Conceptualization (supporting); Methodology (supporting); Writing – review & editing (equal). **Andrey V. Shytov:** Conceptualization (equal); Formal analysis (equal); Investigation (equal); Methodology (supporting); Validation (equal); Writing – review & editing (equal). **Volodymyr V. Kruglyak:** Conceptualization (equal); Formal analysis (supporting); Funding acquisition (lead); Investigation (supporting); Methodology (equal); Project administration (lead); Supervision (lead); Writing – original draft (equal); Writing – review & editing (equal).

DATA AVAILABILITY

The data that support the findings of this study are available within the article and its supplementary material.

REFERENCES

[1]V. V. Kruglyak, S. O. Demokritov, and D. Grundler, "Magnonics," J. Phys. D: Appl. Phys. **43**, 264001 (2010).
[2]A. I. Akhiezer, V. G. Bar'yakhtar, and S. V. Peletminskii, *Spin Waves* (North-Holland, Amsterdam, 1968).
[3]A. Khitun, M. Bao, and K. L. Wang, "Magnonic logic circuits," J. Phys. D: Appl. Phys. **43**, 264005 (2010).
[4]G. Csaba, A. Papp, and W. Porod, "Perspectives of using spin waves for computing and signal processing," Phys. Lett. A **381**, 1471 (2017).
[5]A. V. Chumak, P. Kabos, M. Wu, C. Abert, C. Adelmann, A. O. Adeyeye, J. Åkerman, F. G. Aliev, A. Anane, A. Awad, C. H. Back, A. Barman, G. E. W. Bauer, M. Becherer, E. N. Beginin, V. A. S. V. Bittencourt, Y. M. Blanter, P. Bortolotti, I. Boventer, D. A. Bozhko, S. A. Bunyaev, J. J. Carmiggelt, R. R. Cheenikundil, F. Ciubotaru, S. Cotofana, G. Csaba, O. V. Dobrovolskiy, C. Dubs, M. Elyasi, K. G. Fripp, H. Fulara, I. A. Golovchanskiy, C. Gonzalez-Ballestero, P. Graczyk, D. Grundler, P. Gruszecki, G. Gubbiotti, K. Guslienko, A. Haldar, S. Hamdioui, R. Hertel, B. Hillebrands, T. Hioki, A. Houshang, C.-M. Hu, H. Huebl, M. Huth, E. Iacocca, M. B. Jungfleisch, G. N. Kakazei, A. Khitun, R. Khymyn, T. Kikkawa, M. Kläui, O. Klein, J. W. Kłos, S. Knauer, S. Koraltan, M. Kostylev, M. Krawczyk, I. N. Krivorotov, V. V. Kruglyak, D. Lachance-Quirion, S. Ladak, R. Lebrun, Y. Li, M. Lindner, R. Macêdo, S. Mayr, G. A. Melkov, S. Mieszczak, Y. Nakamura, H. T. Nembach, A. A. Nikitin, S. A. Nikitov, V. Novosad, J. A. Otálora, Y. Otani, A. Papp, B. Pigeau, P. Pirro, W. Porod, F. Porrati, H. Qin, B. Rana, T. Reimann, F. Riente, O. Romero-Isart, A. Ross, A. V. Sadovnikov, A. R. Safin, E. Saitoh, G. Schmidt, H. Schultheiss, K. Schultheiss, A. A. Serga, S. Sharma, J. M. Shaw, D. Suess, O. Surzhenko, K. Szulc, T. Taniguchi, M. Urbánek, K. Usami, A. B. Ustinov, T. van der Sar, S.

Downloaded from http://pubs.aip.org/aip/apl/article-pdf/doi/10.1063/5.0149466/16967078/172403_1_5.0149466.pdf

© Author(s) 2023

van Dijken, V. I. Vasyuchka, R. Verba, S. Viola Kusminskiy, Q. Wang, M. Weides, M. Weiler, S. Wintz, S. P. Wolski, and X. Zhang, "Roadmap on spin-wave computing," IEEE Trans. Magn. **58**, 0800172 (2022).
[6]Y. Au, M. Dvornik, O. Dmytriiev, and V. V. Kruglyak, "Nanoscale spin wave valve and phase shifter," Appl. Phys. Lett. **100**, 172408 (2012).
[7]Y. Au, E. Ahmad, O. Dmytriiev, M. Dvornik, T. Davison, and V. V. Kruglyak, "Resonant microwave-to-spin-wave transducer," Appl. Phys. Lett. **100**, 182404 (2012).
[8]S. Louis, I. Lisenkov, S. Nikitov, V. Tyberkevych, and A. Slavin, "Bias-free spin-wave phase shifter for magnonic logic," AIP Adv. **6**, 065103 (2016).
[9]A. V. Sadovnikov, S. A. Odintsov, E. N. Beginin, S. E. Sheshukova, Y. P. Sharaevskii, and S. A. Nikitov, "Toward nonlinear magnonics: Intensity-dependent spin-wave switching in insulating side-coupled magnetic stripes," Phys. Rev. B **96**, 144428 (2017).
[10]A. B. Ustinov, E. Lähderanta, M. Inoue, and B. A. Kalinikos, "Nonlinear spin-wave logic gates," IEEE Magn. Lett. **10**, 5508204 (2019).
[11]Q. Wang, A. Hamadeh, R. Verba, V. Lomakin, M. Mohseni, B. Hillebrands, A. V. Chumak, and P. Pirro, "A nonlinear magnonic nano-ring resonator," NPJ Comput. Mater. **6**, 192 (2020).
[12]T. Yu and G. E. W. Bauer, "Chiral coupling to magnetodipolar radiation," Top. Appl. Phys. **138**, 1 (2021).
[13]H. Qin, R. B. Holländer, L. Flajšman, F. Hermann, R. Dreyer, G. Woltersdorf, and S. van Dijken, "Nanoscale magnonic Fabry-Pérot resonator for low-loss spin-wave manipulation," Nat. Commun. **12**, 2293 (2021).
[14]K. G. Fripp, A. V. Shytov, and V. V. Kruglyak, "Spin-wave control using dark modes in chiral magnonic resonators," Phys. Rev. B **104**, 054437 (2021).
[15]P. Roberjot, K. Szulc, J. W. Kłos, and M. Krawczyk, "Multifunctional operation of the double-layer ferromagnetic structure coupled by a rectangular nano-resonator," Appl. Phys. Lett. **118**, 182406 (2021).
[16]V. V. Kruglyak, "Chiral magnonic resonators: Rediscovering the basic magnetic chirality in magnonics," Appl. Phys. Lett. **119**, 200502 (2021).
[17]S. R. Lake, B. Divinskiy, G. Schmidt, S. O. Demokritov, and V. E. Demidov, "Microscopic nonlinear magnonic phase shifters based on ultrathin films of a magnetic insulator," Appl. Phys. Lett. **121**, 052403 (2022).
[18]A. Hamadeh, D. Breitbach, M. Ender, A. Koujok, M. Mohseni, F. Kohl, J. Maskill, M. Bechberger, and P. Pirro, "Hybrid magnonic-oscillator system," J. Appl. Phys. **132**, 183904 (2022).
[19]S. Watt, M. Kostylev, A. B. Ustinov, and B. A. Kalinikos, "Implementing a magnonic reservoir computer model based on time-delay multiplexing," Phys. Rev. Appl. **15**, 064060 (2021).
[20]Á. Papp, W. Porod, and G. Csaba, "Nanoscale neural network using non-linear spin-wave interference," Nat. Commun. **12**, 6422 (2021).
[21]M. Kiechle, L. Maucha, V. Ahrens, C. Dubs, W. Porod, G. Csaba, M. Becherer, and Á. Papp, "Experimental demonstration of a spin-wave lens designed with machine learning," IEEE Magn. Lett. **13**, 6105305 (2022).
[22]A. Vansteenkiste, J. Leliaert, M. Dvornik, M. Helsen, F. Garcia-Sanchez, and B. van Waeyenberge, "The design and verification of MuMax3," AIP Adv. **4**, 107133 (2014).
[23]H. Suhl, "Foldover effects caused by spin wave interactions in ferromagnetic resonance," J. Appl. Phys. **31**, 935 (1960).
[24]Y. K. Fetisov, C. E. Patton, and V. T. Synogach, "Nonlinear ferromagnetic resonance and foldover in yttrium iron garnet thin films—Inadequacy of the classical model," IEEE Trans. Magn. **35**, 4511 (1999).
[25]Y. S. Gui, A. Wirthmann, and C.-M. Hu, "Foldover ferromagnetic resonance and damping in permalloy microstrips," Phys. Rev. B **80**, 184422 (2009).
[26]Y. S. Gui, A. Wirthmann, N. Mecking, and C.-M. Hu, "Direct measurement of nonlinear ferromagnetic damping via the intrinsic foldover effect," Phys. Rev. B **80**, 060402 (2009).
[27]V. V. Vitko, A. A. Nikitin, R. V. Haponchyk, A. A. Stashkevich, M. P. Kostylev, and A. B. Ustinov, "Bistable behavior of active ring resonator on surface spin waves," Eur. Phys. J. Plus **137**, 1010 (2022).
[28]S. Fukami and H. Ohno, "Perspective: Spintronic synapse for artificial neural network," J. Appl. Phys. **124**, 151904 (2018).
[29]P. Trempler, R. Dreyer, P. Geyer, C. Hauser, G. Woltersdorf, and G. Schmidt, "Integration and characterization of micron-sized YIG structures with very low Gilbert damping on arbitrary substrates," Appl. Phys. Lett. **117**, 232401 (2020).
[30]L. D. Landau and E. M. Lifshitz, *Mechanics (Course of Theoretical Physics)*, 3rd ed. (Butterworth-Heinemann, Amsterdam, 1976), Vol. 1.
[31]N. N. Bogoliubov and Y. A. Mitropolsky, *Asymptotic Methods in the Theory of Non-Linear Oscillations*, 1st ed. (Gordon and Breach, New York, 1961).

Downloaded from http://pubs.aip.org/aip/apl/article-pdf/doi/10.1063/5.0149466/16967078/172403_1_5.0149466.pdf

© Author(s) 2023